Imaging and three-dimensional reconstruction of chemical groups inside a protein complex using atomic force microscopy

Duckhoe Kim and **Ozgur Sahin**

Departments of Biological Sciences and Physics, Columbia University, New York, USA

Ozgur Sahin: sahin@columbia.edu

Scanning probe microscopes can be used to image and chemically characterize surfaces down to the atomic scale [1–3]. However, the localized tip-sample interactions in scanning probe microscopes limit high-resolution images to the topmost atomic layer of surfaces[1–9], and characterizing the inner structures of materials and biomolecules is a challenge for such instruments. Here, we show that an atomic force microscope can be used to image and three-dimensionally reconstruct chemical groups inside a protein complex. We use short single-stranded DNAs as imaging labels that are linked to target regions inside a protein complex, and T-shaped atomic force microscope cantilevers[10,11] functionalized with complementary probe DNAs allow the labels to be located with sequence specificity and sub-nanometre resolution. After measuring pairwise distances between labels, we reconstruct the three-dimensional structure formed by the target chemical groups within the protein complex using simple geometric calculations. Experiments with the biotin-streptavidin complex show that the predicted three-dimensional loci of the carboxylic acid groups of biotins are within 2-Angstroms of their respective loci in the corresponding crystal structure, suggesting that scanning probe microscopes could complement existing structural biological techniques in solving structures that are difficult to study due to their size and complexity[12].

Recent developments in atomic force microscopy (AFM) techniques are taking advantage of the temporal characteristics of dynamic tip-sample interactions to image material properties with high spatial resolution[11,13–17]. The ability to probe interaction forces with good time resolution also offers the possibility of detecting short-lived biomolecular interactions[18] and harnessing them for chemically specific imaging purposes[19]. DNA hybridization has been investigated previously by AFM[20,21] and even used for DNA-directed molecular manipulation[22]. However, it has not previously been used as imaging labels.

Figure 1a–f illustrates how sequence dependent binding geometries of DNA can, in principle, allow the detection and discrimination of DNA sequences from the temporal characteristics of the forces measured by AFM. The molecular configurations of the probe and targets facilitate the rupture of the orange duplex to be delayed because the single-

stranded green region has to be stretched first. This labelling strategy can be used to image chemical groups within biomolecular complexes and reconstruct their three-dimensional locations (Fig. 1g, h). Although DNA may appear to be an ideal candidate for this labelling strategy, our initial experiments showed that partial hybridization of DNA creates complications, which we had to address (Fig. 2). This is because any unpaired base increases the length of the region that requires stretching, making it difficult to rely on rupture times to discriminate DNA sequences. (We define rupture times relative to the beginning of cantilever oscillation period, which is when the tip is at its highest position).

We minimized the role of partial hybridizations by taking advantage of their reduced lifetimes relative to fully hybridized DNAs. Figure 2a depicts an approximate trend of duplex DNA lifetimes based on previous reports[21,23]. If the lifetime of the partially hybridized DNA were longer than the experiment duration, the measurements would incorporate events that belong to partial hybridizations. However, by choosing a sufficiently short length of DNA, the lifetime of partially hybridized interactions could be kept below the experiment duration, which will minimize the spread of detected rupture times. In agreement with this prediction, our measurements in Fig. 2b exhibit a reduction in the spread of rupture times for 15-, 9-, and 6-base long DNA with sequences listed in Table 1. (To verify that the measured events belong to DNA interactions, we performed control experiments that included blocking the targets and also using non-complementary sequences; Supplementary Section 1.)

After determining that the rupture times of 6-base-long duplex DNAs have sufficient temporal localization, we realized the concept in Fig. 1a–c with a 12-base probe DNA and two 6-base complementary target DNAs (one with sequence A_6 and the other with sequence G_6). As a first step, targets were directly attached to the substrate and not to other biomolecules. Rupture times measured on an A_6-only surface (Fig. 2c) and on a G_6-only surface (Fig. 2d) show that the measured distributions are located in temporally distinct regions of the oscillation period. Furthermore, on a surface with both A_6 and G_6, the distribution of rupture times reproduces a superposition of the original peaks (Fig. 2e). These observations demonstrate that it is possible to rely on rupture times to discriminate short target DNAs.

To explore whether the results in Fig. 2 can be harnessed for chemically specific imaging, we recorded rupture forces (Fig. 3b) and rupture times (Fig. 3c) across a sample of DNA targets immobilized directly onto the substrate, this time with sequences C_6 and T_6. Based on the results in Fig. 2c–e, we first identified locations where rupture forces exceeded the noise threshold value of 39 pN and then examined the corresponding rupture times to determine whether the observed events belonged to the targets (for detailed procedures and selection of the force threshold value, see Methods). Figure 3d shows the resulting multicolour image, which exhibits rupture events that are separated from their nearest neighbours by 0.2 nm to 10 nm. A close examination of this image reveals that several pixels appear as clusters. As we discuss next, these clusters allow the resolution limit and localization accuracy of the imaging system to be estimated.

Figure 3e presents a plot of the distribution of distances from nearest neighbours. The histogram shows that nearly half of the detected events are within a distance of less than 1 nm. The remaining events exhibit a distribution that closely matches the probability distribution function $p(x)$ corresponding to randomly located particles, $p(x) = 2\pi\lambda x e^{-\pi\lambda x^2}$, where λ is the particle density and x is particle spacing[24]. This observation suggests that clustering is not random and comes from repeated measurements of the same target. (We rule out the possibility of multiple probes interacting with targets; for this to explain clustering, probes have to be less than 1 nm apart.)

Statistical analysis of clusters provides valuable information about the resolution limit and the accuracy of the colour assignments. Because clusters originate from repeated rupture events of the same target DNA, the spatial extents observed in the ensemble of clusters (Fig. 3f) represent the point spread function (PSF) of the imaging system for which the full-width at half-maximum (FWHM) corresponds to the resolution limit[25]. We approximated the PSF with a Gaussian profile and averaged the variances (σ^2) calculated for each cluster to estimate the root-mean-square size of the PSF (σ), which is related to the limit of resolution (FWHM ~ 2.4σ)[25]. Along the horizontal and vertical directions, resolution limits are estimated as 0.47 nm ($\sigma = 0.20$ nm) and 0.58 nm ($\sigma = 0.24$ nm), respectively. In addition, the localization accuracy (given as $\sigma/N^{1/2}$, where N is the number of rupture events in a cluster) is better than 0.25 nm (note that the positioning accuracy of the piezoelectric scanner is not included in this estimate). We attribute the extremely small limit of resolution to the small sizes of the probe and target molecules. The contour length of a 6-base-long DNA strand (~ 3.8 nm) is comparable to its persistence length (2 to 3 nm) [26], which would limit the reach of probes and targets.

The colour uniformity of clusters allows the accuracy of colour assignments to be estimated. About 88% of the 299 clusters were completely T_6 or C_6 and only ~4.3% had equal number of T_6 and C_6. The strong correlation between colour assignments within a cluster suggests that interactions between the probe and target DNAs are detected with sequence specificity. Additional experiments with different tip and sample combinations verified the repeatability of the colour uniformities seen in clusters, as well as the resolution limits estimated from the physical sizes of clusters (Supplementary Fig. 2).

We also note that the clusters seen in Fig. 3f are predominantly horizontal. A possible reason for this might be the raster scan pattern of the AFM. While the scanning tip moves continuously in the horizontal direction, it makes discrete steps in the vertical direction. If we consider two cases where a target molecule is located half way between the centres of pixels in the horizontal and vertical directions, the one in the horizontal direction is more likely to be detected because the tip will gradually move over it. Furthermore, this target is likely to be detected as a cluster by appearing in the two adjacent horizontal pixels. In the case of a target located halfway between pixels in the vertical direction, the tip will skip the target as it moves from one scan line to the next. This will lower the probability of the target being detected in adjacent vertical pixels.

After determining the conditions that lead to chemically specific high-resolution images, we used this approach to locate chemical groups within single biomolecules by attaching 6-

base-long single-stranded DNAs to target chemical groups. We worked with the biotin-streptavidin complex. Streptavidin has four binding sites for biotin. Owing to the symmetry of the crystal structure[27], the distance between pairs of carboxylic acids (the sites where DNA labels are linked to biotins) can have three distinct values (Fig. 4a, b). As a result, carboxylic acids of biotins form a tetrahedron with opposite edges having equal length.

Figure 4c, d presents grayscale height images of streptavidin complexed with DNA-labelled biotins, with the locations of detected rupture events highlighted with colour. Twelve additional images are provided in Fig. 4e (Supplementary Figs 3–8 show the entire dataset including control experiments and a separate topography image of a larger area having several streptavidin molecules). Similar to the results in Fig. 3d, we see clustering of rupture events and that these clusters are predominantly composed of single colours, suggesting that colour assignments are accurate even when targets are bound to proteins. Note that although one DNA sequence is sufficient to label biotins, we have nevertheless used two sequences to test if sequences can be discriminated reliably when targets are bound to proteins, which may help with studies of more complex systems.

The images in Fig. 4c–e typically show two distinct locations for rupture events, despite there being four binding sites on streptavidin. This is because only those label DNAs that are oriented towards the tip are likely to bind. Label DNAs that are oriented towards the substrate have to bend in order to hybridize with the probe DNA, which reduces their binding probability (see Supplementary Fig. 9 for more details).

The distance values between the pairs of rupture locations seen in each image exhibit clustering around two values: 5.3 and 6.0 nm (Fig. 4f). A less prominent clustering is seen around 3.0 nm (We noticed that eliminating the images that identify both rupture locations with individual pixels from our statistical analysis reduces the background noise; Supplementary Fig. 10 presents a comparison of raw and filtered versions of the data.) Proceeding with the assumption that these three values reflect the distances between the midpoints of label DNAs (this would be the approximate configuration that requires the least amount of bending energy, as illustrated in Fig. 4g), we first determined the shape of the tetrahedron whose corners correspond to the midpoints of DNA by solving algebraic equations satisfied by the coordinates of the corners. (Note that these equations are satisfied by two mirror symmetric geometries; hereafter we will present results for the solution that matches the symmetry of the crystal structure.) We then estimated the locations of carboxylic acids by translating the corners of the tetrahedron towards its centre of mass by a distance equal to 11 Angstroms (the approximate length of 3-base-long duplex DNA). The new coordinates represent the predicted three-dimensional locations of the carboxylic acids relative to each other. These geometrical calculations involve a number of assumptions. First, we assume the label DNAs would orient approximately normal to the surface of the protein due to electrostatic repulsion and that surface normal can be approximated with the radial line pointing away from the centre of mass. Any errors due to deviations from this approximation would be small because of the short length of the 3-base-long duplex DNA. We also assume that the 6-carbon aliphatic linker that connects DNA to carboxylic acid would orient approximately in the direction of carbons C1 and C3 of the biotin (C1 belongs to the carboxylic acid, and we skipped C2 to account for bond angles in the carbon chain).

This direction is approximately orthogonal to the radial line from the centre of mass[27], so does not contribute to the radial position of labels in a significant way. Furthermore, we neglect deformations of the molecular complex under the applied force, because the peak tapping forces were limited to 10 pN. Graphical illustrations of our calculation steps and further discussions of our key assumptions are given in Supplementary Sections 10 and 11.

Figure 4h and Supplementary Movie 1 show a comparison of the predicted locations of carboxylic acids, represented with yellow spheres, with the crystal structure of the biotin-streptavidin complex. The carboxylic acids in the crystal structure are located at the Y-shaped ends of the red-coloured biotins. To make this comparison we aligned the centre of mass of the predicted three-dimensional geometry and the crystal structure, and then used two of the carboxylic acids in the crystal structure (carbon in the carboxylic acid of the biotins) as reference points to orient the predicted geometry such that the distance between the two references and their two counterparts in the predicted geometry were minimized. As seen in Fig. 4h, despite our crude approximations, there is a good degree of agreement (within 2 Angstroms) between the predicted locations with their counterparts in the crystal structure. This demonstration of the capability to determine three-dimensional locations of chemical groups in biological macromolecules may create a niche for scanning probe microscopes in structural biology where large biomolecular complexes pose significant challenges to existing technologies[12].

Methods

Cantilever design

We used cantilevers with a custom T-shaped geometry introduced previously[10,11,18] (Applied Nanostructures and Bruker-Nano). The cantilever bodies were made of silicon nitride and the tip was made of silicon. The resonance frequencies of the cantilevers in solution were between 4 and 10 kHz (determined from thermal noise spectrum). The spring constant of the vertical deflections range from 35 pN/nm to 200 pN/nm, each calibrated against the thermomechanical noise. The spring constants of the torsional modes (200 pN/nm – 400 pN/nm) were calibrated against the thermal noise spectrum of torsional deflections. This calculation requires the knowledge of tip offset distances, which we determined using scanning electron microscopy. There are variations in the resonance frequencies and spring constants, because we used cantilevers with different lengths. Longer cantilevers provide a better time resolution due to higher ratio of torsional to flexural resonance frequencies (~13.5) compared to the shorter cantilevers (~7), while the shorter cantilevers provide improved signal-to-noise ratio, but underestimate the magnitude of rupture forces due to filtering.

Tip functionalization

We first cleaned the tips by immersing the cantilevers in an acidic solution (nitric acid/H_2O, 1:2) for 20 min. After rinsing with de-ionized water, the tips were dried for overnight under a nitrogen atmosphere. To generate amino groups, the cleaned tips were placed in an anhydrous toluene solution containing 1% APDES (3-aminopropyl diethoxymethyl silane; Gelest) for 3 h under a nitrogen atmosphere. After the reaction, the tips were gently rinsed

with toluene and baked at 95°C for 30 min. The tips were then sequentially washed with toluene, methanol, and deionized water. The resulting amino-functionalized tips were dried in a chamber under a nitrogen atmosphere. Heterofunctional crosslinkers (SM (PEG)$_2$; Thermo Scientific) containing maleimide and *N*-hydroxysuccinimide (NHS) groups at the ends via two ethylene glycol repeats were then applied to the tips to generate a maleimide-functionalized surface. The tips were placed in a crosslinker solution (1mg in 100 μL of PBS, pH 7.4) and incubated for 90 min. After the reaction, the tips were rinsed quentially with PBS buffer, DMSO (methoxy sulfoxide; Sigma Aldrich), and deionized water sequentially. Finally, DNA molecules were immobilized on the surface by placing the tips in a thiolated oligonucleotide solution (Integrated DNA Technologies, 10 μM in PBS) overnight. After incubation, the tips were washed with PBS and deionized water.

Note that our tip functionalization method does not ensure that there will be a single DNA probe at the tip. However, due to the small sizes of probes and targets, probes that are further away from the very end of tip will have a significantly lower probability of binding. There will be an energy barrier imposed by the stretching of the probe, which will reduce binding probability.

DNA surface preparation

Silicon wafer was used as a substrate, and cleaning and modification procedures were applied as for the tip functionalization. To create samples with mixed target sequences, the final concentration of each DNA sequence was adjusted to 5 μM (Supplementary Fig. 2a) or 10 μM (Fig. 3d, Supplementary Fig. 2b, c). After preparation, the substrate was mounted on an AFM sample stage for imaging. Imaging was performed in PBS (pH 7.4).

DNA-bound biotin-streptavidin sample preparation

A stock solution of streptavidin (Sigma Aldrich) was prepared in 1mg ml^{-1} PBS (pH 6.8) and diluted it with PBS (pH 6.8) to a final concentration of 0.1 mg mL^{-1} for each experiment. A volume of 60 uL of diluted solution was dropped onto a freshly cleaved mica surface (VWR). After 1 h, the mica surface was washed with PBS (pH 6.8) and subsequently incubated overnight in a solution containing DNA targets modified with a biotin at its 5′ end (Integrated DNA technologies; 10 μM for each target in PBS, pH 6.8). After the incubation, the surface was washed with PBS (pH 6.8) and mounted on the AFM sample stage for imaging. Imaging was performed in PBS (pH 6.8).

Imaging

AFM experiments were performed with two commercial AFM systems (BioScope II and Multimode V, Bruker-Nano, Inc.), and imaging was carried out in fluid tapping mode at room temperature (20 °C). Torsional deflection signals from T-shaped cantilevers were analyzed in real time to create rupture force and rupture time maps. Rupture force is defined as the minimum value (most negative) of the tip-sample force waveform, and rupture time is defined as the temporal location of the minimum force value within a single oscillation period. The highest point of the tip determines the beginning and ending of the period. The analysis was carried out in Labview (National Instruments) with a computer equipped with a data acquisition card (NI-S6115). We used previously described algorithms to calculate tip-

sample force waveforms[18]. During imaging, the drive amplitudes were adjusted to maintain peak tapping forces to below 10 pN, which can be expected to minimize the deformations of the protein surface. The set-point amplitudes were selected according to the length of DNA molecules. For the experiments in Fig. 2, to account for differences in the contour lengths of 6-, 9-, and 15-base-long DNA, the peak-to-peak oscillation amplitudes were adjusted in proportion to the number of bases and approximately equal to twice the contour length of hybridized DNA. We used 0.63 nm/base to approximate the contour length[26]. For multicolor imaging, the set-amplitude value was maintained at ~4 nm. The immobilized DNA surface was imaged with a scan speed of 400 nm/sec. To image streptavidin molecules complexed with biotinylated DNA, scan speeds of ~600 to 1000 nm/sec were used.

Note that we occasionaly observed tip contaminations during the imaging. The contaminants altered the attractive forces between the tip and sample and appeared as increased adhesiveness. However, it was not prohibitive because most contaminated tips recovered the typical adhesive force level while imaging.

To identify the locations of rupture events, we determined a threshold force level beyond which a measured pulling force is considered as a rupture event between the complementary probe and target. To achieve this, we compared force histograms recorded on fully complementary targets and non-complementary targets and selected the value beyond which the events counted on non-complementary surface were less than 5% of the events counted on a complementary DNA surface. The resulting error rate of 5% represents a compromise in minimizing false positives (selectivity) and false negatives (sensitivity). The threshold value were 12 – 14 pN for Fig. 2 and Supplementary Fig. 2a, b and 39 – 49 pN for Fig. 4 and Supplementary Fig. 2c, and 3–7. Note that the limited torsional bandwidth of the shorter T-shaped cantilevers used in the experiments underestimates the rupture forces. Because the binding probability of probe and targets is low, we incorporated rupture data from trace and retrace images into a single image for experiments on immobilized DNA samples. For DNA labels bound to biotin-streptavidin complexes, we used trace and retrace images separately. By comparing the locations of the rupture events in trace and retrace images on DNA surfaces, we found that approximately 50% of events overlap (within 2 nm) with a rupture event in the other image. This suggests that the probability of detecting a single label in a single image is about 50% (see Supplementary Information for additional discussion). Therefore, combining rupture data from both images would allow the detection of a majority of the labels.

To determine whether a detected rupture event corresponds to one or the other target, we looked at the rupture time. We defined the length of the entire period as 64 units (ranging from −32 to 32, with zero corresponding to the lowest point of the tip). Based on the results in Fig. 2c–e, rupture events between −10 and 10 are counted as the target complementary to the base region of the DNA probe and events between 18 and 32 are counted as the target complementary to the free end of the DNA probe. Once the target was determined, a colour-coded image was generated.

Image analysis

With the immobilized DNA samples, we determined clusters in rupture events and characterized the spread of each cluster. We defined clusters such that a given pixel representing a rupture event belongs to a cluster if at least one of the elements of the cluster is within 0.68 nm (3.5 pixels). This threshold is determined by the histogram in Fig. 3e. With this algorithm we identified 299 clusters. The variances in horizontal and vertical directions were calculated for each cluster using sample means. For clusters with more than two elements, the computer picked two elements randomly. The resulting variance was averaged over the entire set of clusters. If a cluster has elements only in the same row or column, its variance is not included in the calculations for the orthogonal direction. With the biotin-streptavidin complexes, we analysed the distances between the rupture locations. In the case of clustered pixels, we assumed the rupture location was at the centre of mass of the cluster. We ignored rupture signals that fell outside of the boundaries of streptavidin, as these may be caused by force noise or unspecific interactions. Pairwise distance data were analyzed by calculating the density of data points as a function of distance. A moving window that was 0.5 nm wide was used in the density calculations.

Supplementary Material

Refer to Web version on PubMed Central for supplementary material.

Acknowledgments

References

1. Giessibl FJ, Hembacher S, Bielefeldt H, Mannhart J. Subatomic features on the silicon (111)-(7 × 7) surface observed by atomic force microscopy. Science. 2000; 289:422–425. [PubMed: 10903196]

2. Sugimoto Y, et al. Chemical identification of individual surface atoms by atomic force microscopy. Nature. 2007; 446:64–67. [PubMed: 17330040]

3. Gross L, Mohn F, Moll N, Liljeroth P, Meyer G. The chemical structure of a molecule resolved by atomic force microscopy. Science. 2009; 325:1110–1114. [PubMed: 19713523]

4. San Paulo A, Garcia R. High-resolution imaging of antibodies by tapping-mode atomic force microscopy: attractive and repulsive tip-sample interaction regimes. Biophys J. 2000; 78:1599–1605. [PubMed: 10692344]

5. Ido S, et al. Beyond the Helix Pitch: Direct Visualization of Native DNA in Aqueous Solution. ACS nano. 2013; 7:1817–1822. [PubMed: 23350676]

6. Cerreta A, Vobornik D, Dietler G. Fine DNA Structure Revealed by Constant Height Frequency Modulation AFM Imaging. Eur Polym J. 2013; 49:1916–1922.

7. Ido S, et al. Immunoactive two-dimensional self-assembly of monoclonal antibodies in aqueous solution revealed by atomic force microscopy. Nature Mater. 2014; 13:264–270. [PubMed: 24441879]

8. Müller DJ, Fotiadis D, Scheuring S, Müller SA, Engel A. Electrostatically balanced subnanometer imaging of biological specimens by atomic force microscope. Biophys J. 1999; 76:1101–1111. [PubMed: 9916042]

9. Voïtchovsky K, Kuna JJ, Contera SA, Tosatti E, Stellacci F. Direct mapping of the solid-liquid adhesion energy with subnanometre resolution. Nature Nanotech. 2010; 5:401–405.

10. Dong M, Husale S, Sahin O. Determination of protein structural flexibility by microsecond force spectroscopy. Nature Nanotech. 2009; 4:514–517.

11. Sahin O, Magonov S, Su C, Quate CF, Solgaard O. An atomic force microscope tip designed to measure time-varying nanomechanical forces. Nature Nanotech. 2007; 2:507–514.

12. Jones N. Crystallography: Atomic secrets. Nature. 2014; 505:602. [PubMed: 24476871]

13. Jesse S, Kalinin SV, Proksch R, Baddorf A, Rodriguez B. The band excitation method in scanning probe microscopy for rapid mapping of energy dissipation on the nanoscale. Nanotechnology. 2007; 18:435503.

14. Garcia R, Herruzo ET. The emergence of multifrequency force microscopy. Nature Nanotech. 2012; 7:217–226.

15. Xu X, Melcher J, Basak S, Reifenberger R, Raman A. Compositional contrast of biological materials in liquids using the momentary excitation of higher eigenmodes in dynamic atomic force microscopy. Phys Rev Lett. 2009; 102:060801. [PubMed: 19257574]

16. Platz D, Forchheimer D, Tholén EA, Haviland DB. Interaction imaging with amplitude-dependence force spectroscopy. Nat Commun. 2013; 4:1360. [PubMed: 23322048]

17. Tetard L, Passian A, Thundat T. New modes for subsurface atomic force microscopy through nanomechanical coupling. Nature Nanotech. 2010; 5:105–109.

18. Dong M, Sahin O. A nanomechanical interface to rapid single-molecule interactions. Nat Commun. 2011; 2:247. [PubMed: 21427718]

19. Hinterdorfer P, Dufrene YF. Detection and localization of single molecular recognition events using atomic force microscopy. Nat Methods. 2006; 3:347–355. [PubMed: 16628204]

20. Lee GU, Chrisey LA, Colton RJ. Direct measurement of the forces between complementary strands of DNA. Science. 1994; 266:771–773. [PubMed: 7973628]

21. Strunz T, Oroszlan K, Schäfer R, Güntherodt HJ. Dynamic force spectroscopy of single DNA molecules. Proc Natl Acad Sci USA. 1999; 96:11277–11282. [PubMed: 10500167]

22. Kufer SK, Puchner EM, Gumpp H, Liedl T, Gaub HE. Single-molecule cut-and-paste surface assembly. Science. 2008; 319:594–596. [PubMed: 18239119]

23. Cocco S, Monasson R, Marko JF. Force and kinetic barriers to initiation of DNA unzipping. Phys Rev E. 2002; 65:041907.

24. Bansal P, Ardell A. Average nearest-neighbour distances between uniformly distributed finite particles. Metallography. 1972; 5:97–111.

25. Pertsinidis A, Zhang Y, Chu S. Subnanometre single-molecule localization, registration and distance measurements. Nature. 2010; 466:647–651. [PubMed: 20613725]

26. Murphy M, Rasnik I, Cheng W, Lohman TM, Ha T. Probing single-stranded DNA conformational flexibility using fluorescence spectroscopy. Biophys J. 2004; 86:2530–2537. [PubMed: 15041689]

27. Stenkamp RE, Trong IL, Klumb L, Stayton PS, Freitag S. Structural studies of the streptavidin binding loop. Prot Sci. 1997; 6:1157–1166.
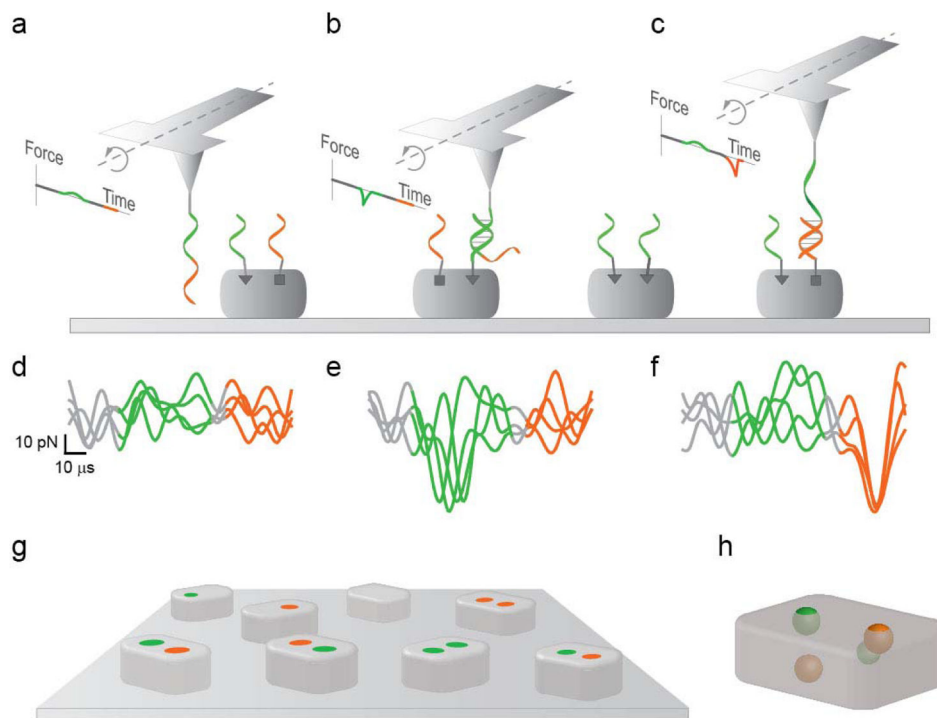
Fig. 1. Chemically-specific imaging and 3-D reconstruction using DNA labels
(a–c) A strand of DNA (probe) interacts with target DNA strands with shorter sequences.
Sequences of target DNAs are complementary to different regions along the probe DNA
(complementary sequences are given in identical colours). Formation of duplexes creates
distinct force-time waveforms, which are detected by the twisting of T-shaped AFM
cantilevers. The pulling forces exerted by the target molecules appear as negative peaks in
the force-time waveforms. (d–f) Examples of experimentally measured waveforms
corresponding to three cases in (a–c). Mapping the timing of pulling events across the
sample surface allows locating specific chemical targets with high spatial-resolution (g) and
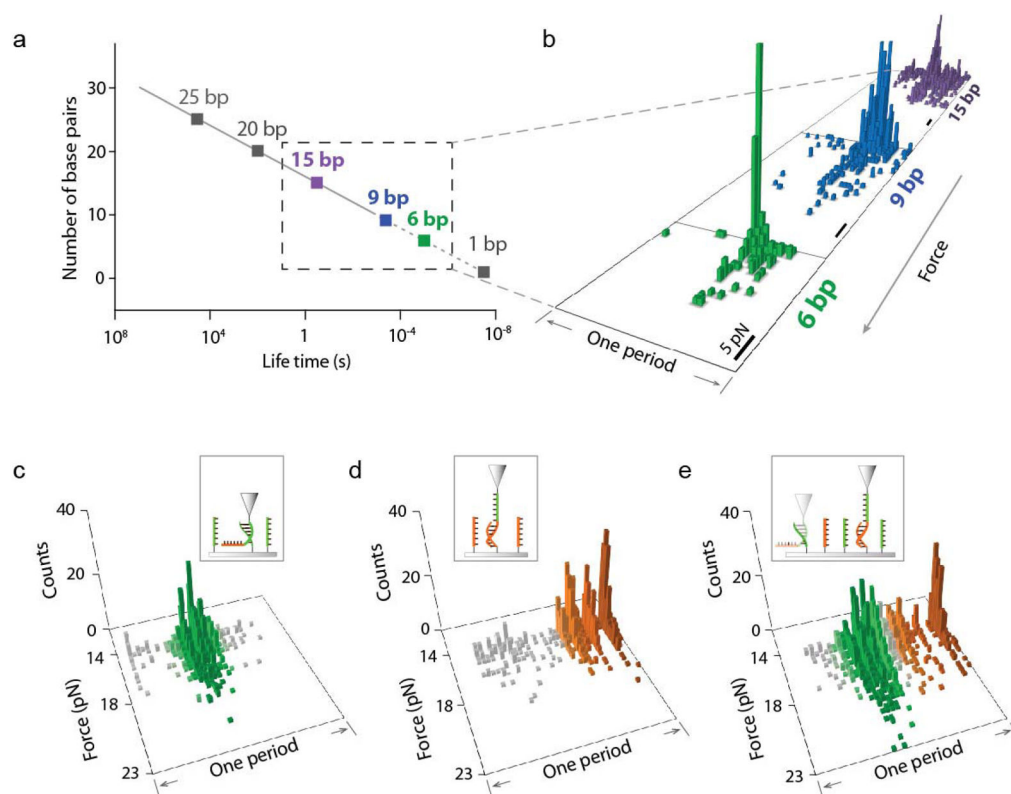reconstructing the 3-D locations of targets from their pairwise distances (h).

Fig. 2. Tuning the lifetime of DNA interactions enhances target specificity
(a) Approximate lifetimes of DNA duplexes as a function of complementary bases[21,23]. (b) Distribution of measured rupture forces and times plotted for 15-, 9-, and 6-base long complementary DNA (time is given relative to the oscillation period). (c, d) Distribution of measured rupture forces and times on samples containing either A_6 (c) or G_6 (d). Insets: Probe and target configurations. (e) Distribution measured on a sample containing both targets reproduced the peaks in (c, d). Orange, green, and grey columns in (c–e) indicate regions corresponding to each target (orange and green) and regions where a decision cannot be made (grey).
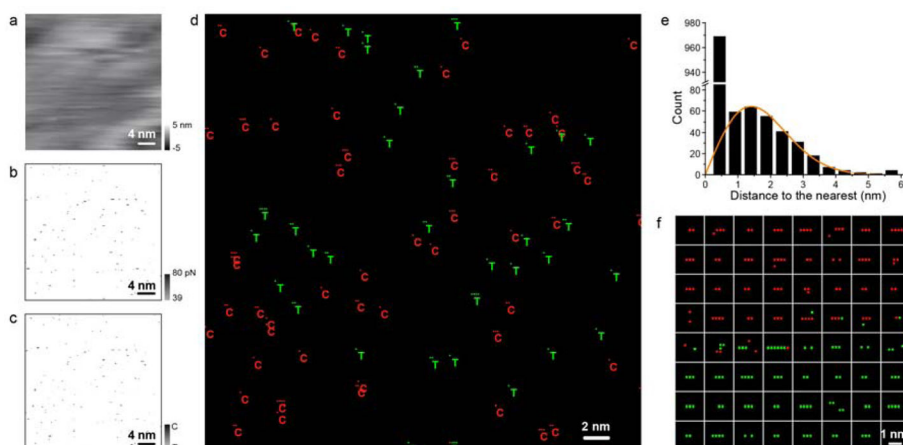
Fig. 3. Multicolour imaging of target DNA molecules
(a) Topographic image of a surface with immobilized single-stranded DNAs. Due to the small size of targets (6 bases long), the topographic image does not exhibit noticeable features of target DNAs. (b) Simultaneously recorded map of locations where pulling forces exceed the predetermined noise threshold. Forces are given in grayscale in proportion to their difference from the threshold value. (c) Rupture times at the locations identified in (b) to be above the threshold. Rupture times are given in grayscale and are scaled between the beginning (white) and the end (black) of the oscillation period, when the tip is at the highest points of its trajectory. (d) Results colour-coded according to the values of rupture times according to Fig. 2(c–e) and marked with letters C and T. (e) Distribution of the distances between nearest neighbours in the sample imaged in (d). The orange curve represents the probability distribution function corresponding to randomly located particles. (f) A selection of clustered probe-target interactions showing the variety in their arrangements and colour patterns. Clusters are defined as groups of colored pixels, in which each colored pixel is at most 0.68 nm away from its nearest neighbor. Clusters in a 100 nm × 100 nm region were found by the computer and plotted as separate images in each small square region in (f).
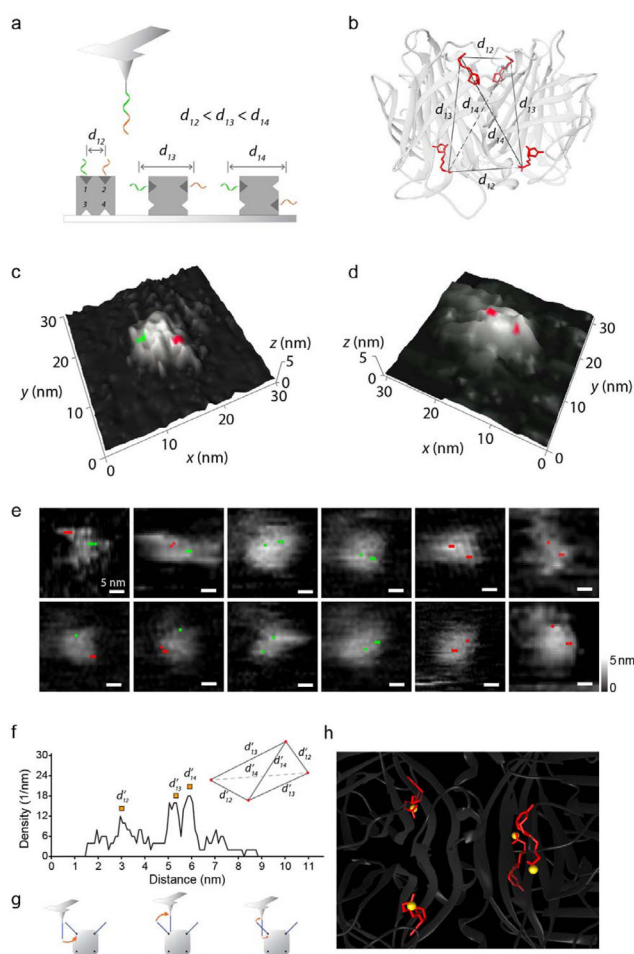
Fig. 4. Chemically specific imaging and 3-D reconstruction in a protein complex

(a) Illustration of biotin-streptavidin complexes formed with 6-base-long biotinylated DNA. Biotin-to-biotin distances are denoted d_{12}, d_{13}, d_{14}. (b) Crystal structure of the biotin-streptavidin complex[27], with biotins highlighted in red. (c, d) 3-D rendered topographic images of two biotin-streptavidin complexes with the locations of rupture events marked with colour. (e) Additional images from twelve different complexes (locations of rupture events are overlaid with grayscale topography images). (f) Density-based cluster analysis of the measured distances from 34 unique complexes (density of data points is calculated with a moving window of 0.5 nm). We assumed that the three values marked by orange squares correspond to the edges of a tetrahedron formed by the DNA labels. (g) Relative positions of probe and target DNAs affect binding probabilities. The most likely binding can be expected to occur when the middle points of hybridizing strands roughly align. (h) Overlay of the predicted locations of carboxylic acids of biotins (yellow spheres) with the crystal structure. The horizontal field of view is approximately 4 nm.

Table 1

Probe and target DNA sequences.

	Probe	Target(s)
Figure 2b (**15-bp**)	5′-SH-ACC TGA CCC GGG TTT -3′	5′-SH-AAA CCC GGG TCA GGT-3′
Figure 2b (**9-bp**)	5′-SH-CCC GGG TTT-3′	5′-SH-AAA CCC GGG-3′
Figure 2b (**6-bp**) Figure S1a	5′-SH-GGG TTT-3′	5′-SH-AAA CCC-3′
Figure S1b	5′-SH-GGG TTT-3′	5′-SH-GGG TTT-3′
Figure 2c–e Figure S2a	5′-SH-TTT TTT CCC CCC-3′	5′-SH-AAA AAA-3′
		5′-SH-GGG GGG-3′
Figure 3d Figure S2b, S2c	5′-SH-AAA AAA GGG GGG-3′	5′-SH-TTT TTT-3′
		5′-SH-CCC CCC-3′
Figure 4 Figure S3, S5–S7	5′-SH-AAA AAA GGG GGG-3′	5′-biotin-TTT TTT-3′
		5′-biotin-CCC CCC-3′
Figure S4	5′-SH-AAA AAA GGG GGG-3′	5′-biotin-AAA AAA-3′
		5′-biotin-GGG GGG-3′